

Observational Techniques for Detecting Planets in Binary Systems

Matthew W. Muterspaugh, Maciej Konacki, Benjamin F. Lane, and Eric Pfahl

1 Why Focus Planet Searches on Binary Stars?

Searches for planets in close binary systems explore the degree to which stellar multiplicity inhibits or promotes planet formation. There is a degeneracy between planet formation models when only systems with single stars are studied—several mechanisms appear to be able to produce such a final result. This degeneracy is lifted by searching for planets in binary systems; the resulting detections (or evidence of non-existence) of planets in binaries isolates which models may contribute to how planets form in nature. Studying relatively close pairs of stars, where dynamic perturbations are the strongest, provides the most restrictive constraints of this type [see, for example, Thébault et al., 2004, Pfahl, 2005, Pfahl and Muterspaugh, 2006].

In this chapter, we consider observational efforts to detect planetary companions to binary stars in two types of hierarchical planet-binary configurations: first “S-type” planets which orbit just one of the stars, with the binary period being much longer than the planet’s; second, “P-type” or circumbinary planets, where the planet simultaneously orbits both stars, and the planetary orbital period is much longer than that of the binary [Dvorak, 1982]. Simulations show each of these configurations has a large range of stable configurations [see, e.g., Benest, 2003, Pilat-Lohinger et al., 2003, Pilat-Lohinger and Dvorak, 2002, Broucke, 2001, Holman and Wiegert, 1999, Benest, 1996, 1993, 1989, 1988, Rabl and Dvorak, 1988, also, this book, chapters ZZZZ].

2 S-Type Planets

S-Type planets orbit just one of the stars in a binary, and the binary separation is much larger than that between the star and planet. Some of the binaries are so widely separated (projected semimajor axis $a_b \gtrsim 1$ arcsecond) that they can be spatially resolved by ground-based telescopes without active image correction; for these, traditional planet-finding techniques can

be used. In fact, astrometric methods often perform best in this regime, as the secondary star serves as a convenient reference for the primary, and vice versa. Here, astrometric and radial velocity (RV) programs are considered as the most versatile search methods. (While transit searches might also be possible, these typically have very limited spatial resolutions, and the second star can act as a photometric “contaminant.”) When the binaries are not spatially resolved with simple imaging, modifications must be made to meet the measurement precisions required for detecting extrasolar planets.

2.1 Wide Binaries

From an observational standpoint, “wide” binaries are considered to be those that can be resolved by traditional (uncorrected) imaging techniques. Due to atmospheric seeing, this sets the projected sky separation at larger than roughly one arcsecond.

2.1.1 Dualstar Astrometry

Interferometric narrow-angle astrometry [Shao and Colavita, 1992, Colavita, 1994] promises astrometric performance at the 10-100 micro-arcsecond level for pairs of stars separated by 1-60 arcseconds. The lower limit of the allowable binary separation for this technique is that the binary is resolved by the individual telescopes in the interferometer; the upper limit is set by the scale over which the effects of atmospheric turbulence are correlated. This technique was first demonstrated with the Mark III interferometer for short integrations [Colavita, 1994], was extended to longer integrations and shown to work at the 100 micro-arcsecond level at the Palomar Testbed Interferometer [PTI, Lane et al., 2000].

However, achieving such performance requires simultaneous measurement of the interferometric fringe positions of both stars, greatly complicating the instrument (two beam combiners and metrology throughout the entire array are required). In addition, the instrumental baseline vector \vec{B} connecting the unit telescopes must be known to high precision (≈ 100 microns).

In an optical interferometer light is collected at two or more apertures and brought to a central location where the beams are combined and a fringe pattern produced on a detector. For a broadband source of central wavelength λ and optical bandwidth $\Delta\lambda$ the fringe pattern is limited in extent and appears only when the optical paths through the arms of the interferometer

are equalized to within a coherence length ($\Lambda = \lambda^2/\Delta\lambda$). For a two-aperture interferometer, neglecting chromatic dispersion by unequal air paths, the intensity measured at one of the combined beams is given by

$$I(x) = I_0 \left[1 + V \frac{\sin(\pi x/\Lambda)}{\pi x/\Lambda} \sin(2\pi x/\lambda) \right] \quad (1)$$

where V is the fringe contrast or “visibility”, which can be related to the morphology of the source, and x is the optical path difference between arms of the interferometer; see Fig. 1. More detailed analysis of the operation of optical interferometers can be found in *Principles of Long Baseline Stellar Interferometry* [Lawson, 2000].

The location of the resulting interference fringes are related to the position of the target star and the observing geometry via

$$d = \vec{B} \cdot \vec{S} + \delta_a(\vec{S}, t) + c \quad (2)$$

where d is the optical path-length one must introduce between the two arms of the interferometer to find fringes (often called the “delay”), \vec{S} is the unit vector in the source direction, and c is a constant additional scalar delay introduced by the instrument. The term $\delta_a(\vec{S}, t)$ is related to the differential amount of path introduced by the atmosphere over each telescope due to variations in refractive index.

If the other quantities are known or small, measurement of the instrumental path length d required to observe fringes determines the position of the star \vec{S} . For a 100-m baseline interferometer, an astrometric precision of 10 μas corresponds to knowing d to 5 nm, a difficult but not impossible proposition for all terms except that related to the atmospheric delay. Atmospheric turbulence, which changes over distances of tens of centimeters and on millisecond timescales, forces one to use very short exposures to maintain fringe contrast, and hence limits the sensitivity of the instrument. It also severely limits the astrometric accuracy of a simple interferometer, at least over large sky-angles.

However, in narrow-angle astrometry one is concerned with a close pair of stars, and the observable is a differential astrometric measurement, i.e. one is interested in knowing the angle between the two stars ($\vec{\Delta}_s = \vec{s}_2 - \vec{s}_1$). The atmospheric turbulence is correlated over small angles. If the measurements of the two stars are simultaneous, or nearly so, the atmospheric term subtracts out making possible high precision “narrow-angle” astrometry.

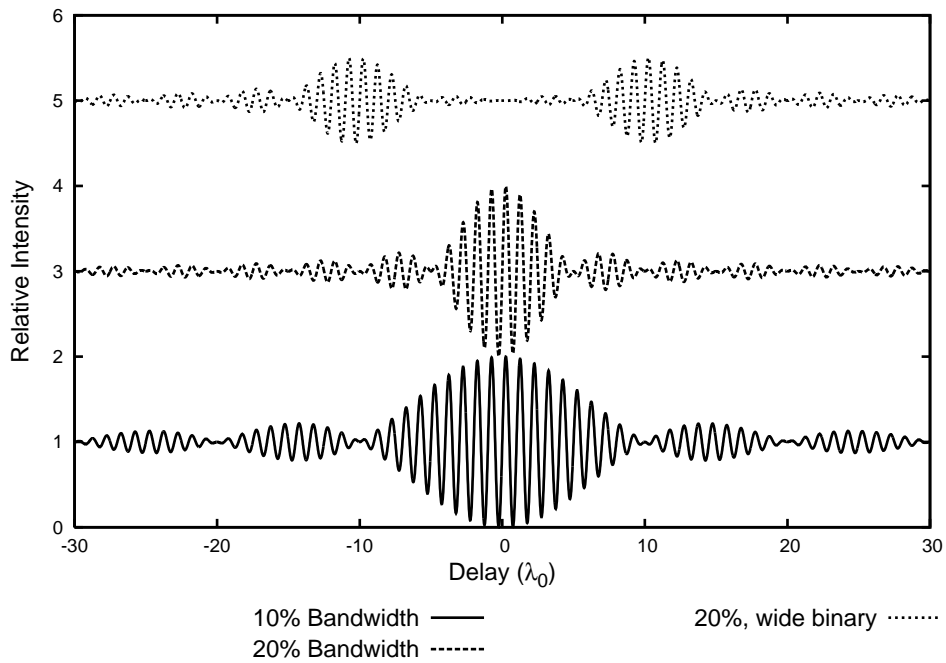


Figure 1: The response of an interferometer. The top two curves have been offset by 2 and 4 for clarity. The widths of the fringe packets are determined by the bandpass of the instrument, and the wavelength of fringes by an averaged wavelength of starlight. The top curve shows the intensity pattern obtained by observing two stars separated by a small angle on the sky—the observable is the distance between the fringe packets.

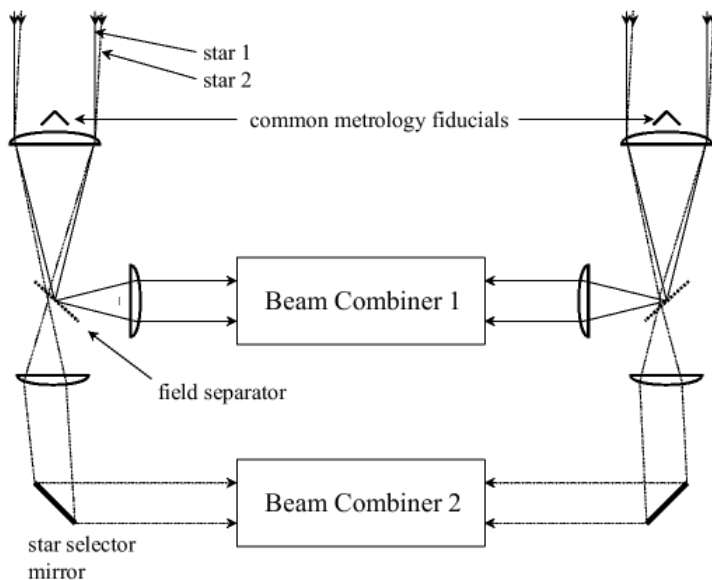


Figure 2: Schematic of splitting the light in a dualstar interferometer.

The requirement that the target and reference stars be observed simultaneously results in a significant instrumental complexity, i.e. essentially two complete interferometers are required to share the same set of apertures (see Fig. 2). The splitting of light from the stars into two separate sets of delay lines, beam transport systems and beam combiners is done in a “dual-star module” located just after the apertures, with the split generally being accomplished using a beam-splitter. Considerable care must be taken in designing the system in order to avoid small pathlength measurement errors.

The exact level of astrometric precision that can be achieved depends on many factors, including the separation of the target/reference pair, the size of the interferometric baseline and the levels and distribution of atmospheric turbulence. For a typical Mauna Kea seeing profile the astrometric precision is

$$\sigma_a \simeq 300 \frac{\theta}{\sqrt{t} B^{2/3}} \text{ arcsec} \quad (3)$$

where B is the baseline length in meters, θ is the target/reference separation in radians, and t is the integration time in seconds. For typical baselines of ~ 100 m, and an angular separation of ~ 30 arcsecond implies an astrometric

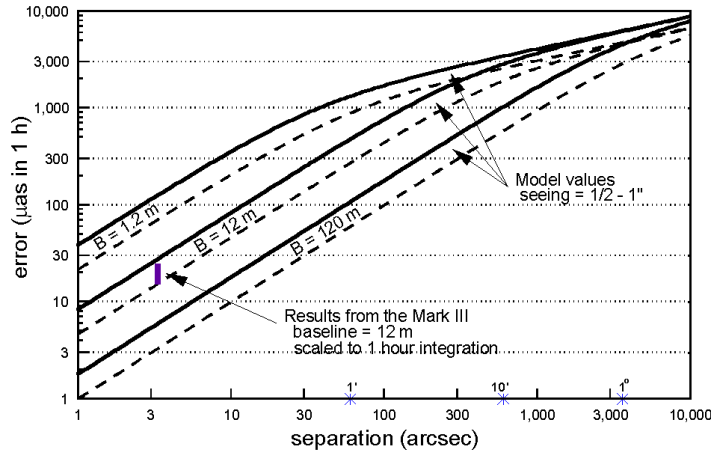


Figure 3: Astrometric accuracy vs. star separation in a one-hour integration for different baseline lengths. Model atmospheres providing 1/2- and 1.0-arcsecond seeing are shown. These results assume an infinite outer scale, and better results are achieved when the baseline exceeds the outer scale, as would be expected with a 100 m baseline at most sites. Measurements with the Mark III interferometer of a 3.3 arcsecond binary star are consistent with the model. This figure is from Shao and Colavita [1992].

precision of $30 \mu\text{as}$ in an hour (see Fig. 3).

The magnitude of the astrometric signal of the star's motion about the center of mass (CM) between it and its planet is given by:

$$\Delta a_{CM} = 2 \frac{M_p}{M_s} a_p = \frac{M_p/M_J}{M_s/M_\odot} \frac{a_p}{524}. \quad (4)$$

where M_p , M_b , M_J , M_\odot are, respectively, masses of the planet, star, Jupiter, and Sun, and a_p is the semimajor axis of the planet's orbit.

Thus, the minimum mass that can be detected is roughly

$$M_p/M_J \gtrsim 524 \frac{\sigma_a}{a_p} \frac{M_s}{M_\odot} \quad (5)$$

$$\gtrsim 0.1 \frac{\sigma_a/20\mu\text{as}}{a_p/1\text{AU}} \frac{d}{10\text{pc}} \frac{M_s}{M_\odot} \quad (6)$$

$$M_p/M_\oplus \gtrsim 1.6 \frac{\sigma_a/1\mu\text{as}}{a_p/1\text{AU}} \frac{d}{10\text{pc}} \frac{M_s}{M_\odot} \quad (7)$$

where M_\oplus is the mass of the Earth, and here d is the distance to the target star.

2.1.2 Radial Velocities

When the stars in a binary can be spatially resolved without active image correction on ground based telescopes, the spectrum of each star can be recorded separately without contamination from the other, and the standard precision RV method described below can be used [see, for example, Campbell et al., 1988, Butler et al., 1996]. Similarly, if the secondary is much fainter than the primary, precision RV might be performed on the brighter star as though it were single, though there is concern about the influence of the fainter lines. Several (~ 30) exoplanet candidates in binaries have been discovered in this manner. In some cases the stars were not previously known to be binaries, and their natures were only discovered by long-term RV trends or follow-up adaptive optics imaging. Some of these efforts to detect planets in binary stellar systems include that of Toyota et al. [2005] for single-lined and wide binaries, that of Desidera et al. [2006] targeting wide binaries, and the program targeting single-lined and wide binaries of Udry et al. [2004].

The highest precision RV observations are obtained either from the I_2 (molecular iodine) absorption cell or the use of carefully designed spectrographs with fiber scrambling. In order to achieve a RV precision of $\sim 1\text{ m s}^{-1}$ an iodine absorption cell is used to superimpose a reference spectrum on the stellar spectrum (by sending a starlight through the cell). The spectrum provides a fiducial wavelength scale against which radial velocity shifts are measured.

Thanks to its conceptual simplicity, the iodine technique is the most commonly adopted way to obtain precision radial velocities. Iodine absorption cells are available on many spectrographs—HIRES at the 10m Keck I (Keck

Observatory), Hamilton at the 3m Shane (Lick Observatory), SARG at the 3.6m TNG (Canary Islands), UCLES at the 3.9m Anglo-Australian Telescope (Anglo-Australian Observatory), HRS at the 9m HET (McDonald Observatory), MIKE at the 6.5m Magellan (Las Campanas Observatory), UVES at the 8m Kueyen (Cerro Paranal), HDS at the 8.2m Subaru (National Astronomical Observatory of Japan) and many other—and are used for planet detections.

In the iodine absorption cell technique, the Doppler shift of a star spectrum is determined by solving the following equation [Marcy and Butler, 1992]

$$I_{obs}(\lambda) = [I_s(\lambda + \Delta\lambda_s) T_{I_2}(\lambda + \Delta\lambda_{I_2})] \otimes PSF \quad (8)$$

where $\Delta\lambda_s$ is the shift of the star spectrum, $\Delta\lambda_{I_2}$ is the shift of the iodine transmission function T_{I_2} , \otimes represents a convolution, and PSF a spectrograph's point-spread function. The parameters $\Delta\lambda_s, \Delta\lambda_{I_2}$ as well as parameters describing the PSF are determined by performing a least-squares fit to the observed spectrum, I_{obs} , as seen through the iodine cell. To this end, one also needs a high SNR star spectrum taken without the cell, I_s , which serves as a template for all the spectra observed through the cell, as well as the I_2 transmission function, T_{I_2} , obtained with the Fourier Transform Spectrometer at the Kitt Peak National Observatory. The Doppler shift of a star spectrum is then given by $\Delta\lambda = \Delta\lambda_s - \Delta\lambda_{I_2}$.

The velocity reflex amplitude of a star due to an unseen companion is given by

$$\begin{aligned} \Delta v_b &= 2 \frac{2\pi a_p \sin i_p}{P_p} \frac{M_p}{M_s + M_p} = \frac{2\sqrt{G} M_p \sin i_p}{\sqrt{(M_s + M_p) a_p}} \\ &= 56.9 \text{ m s}^{-1} \times \frac{(M_p \sin i_p / M_J)}{\sqrt{((M_s + M_p) / M_\odot) (a_p / 1\text{AU})}} \end{aligned} \quad (9)$$

where P_p is the period of the planet's orbit, G is the gravitational constant, and i_p is the inclination of the planet's orbit.

For an RV precision of σ_{rv} , the minimum mass that can be detected is roughly

$$M_p \sin i_p / M_J \gtrsim 0.018 \frac{\sigma_{rv}}{1 \text{ m s}^{-1}} \sqrt{((M_s + M_p) / M_\odot) (a_p / 1\text{AU})} \quad (10)$$

$$M_p \sin i_p / M_\oplus \gtrsim 5.6 \frac{\sigma_{rv}}{1 \text{ m s}^{-1}} \sqrt{((M_s + M_p) / M_\odot) (a_p / 1\text{AU})}. \quad (11)$$

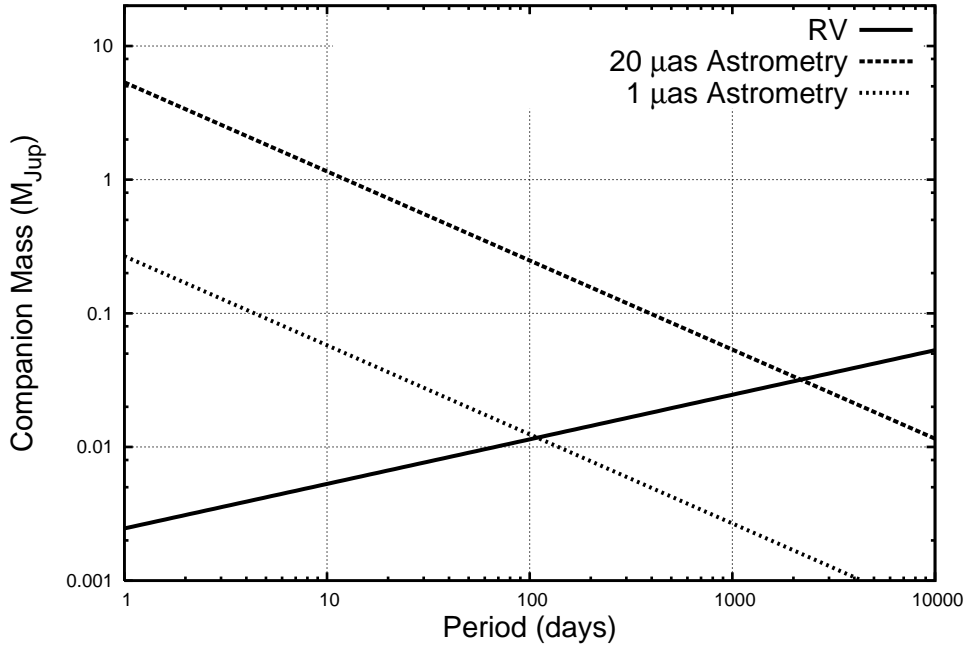


Figure 4: Sensitivity to S-Type planets in wide binaries, comparing astrometric and radial velocity techniques. All calculations assume solar mass stars; astrometric sensitivity assumes a distance of 10 pc to the target system.

2.1.3 Observational Precisions

Astrometry is most sensitive to long period planets, RV to short period ones. Figure 4 shows the companion masses one can detect for each method, assuming $20 \mu\text{as}$ ground-based astrometry, $1 \mu\text{as}$ space-based astrometry, and 1m s^{-1} RV precisions.

2.2 Close Binaries

Radial velocity surveys for extrasolar planets have been restricted largely to stars within $\simeq 100$ pc, and the majority of detected exoplanets are at distances of 10–50 pc. Therefore, our observational definition of a “wide” binary corresponds to projected orbital separations of $\gtrsim 50$ AU. More compact systems form the complementary class of “close” binaries. From a theoretical standpoint, binaries with semimajor axes of $\lesssim 50$ AU pose important challenges to

standard ideas about the formation of giant planets.

Imagine a protoplanetary disk around one star in a newly formed binary. Suppose that the orbit has semimajor axis a and eccentricity e , and assume, for simplicity, that the stars have equal masses. The tidal gravitational field of the companion star truncates the disk at a radius of $R_t \simeq 0.26a(1 - e^2)^{1.2}$ [e.g. Pichardo et al., 2005]. If $R_t \lesssim 3$ AU (i.e., inside the so-called “ice line”), it seems unlikely that icy grains could form and grow into planetesimals, thus precluding the embryonic stage of giant planet formation in the core-accretion scenario [e.g., Lissauer, 1993]. In more extreme cases, when $R_t \lesssim 1$ AU, there may be insufficient material in the disk to yield a Jovian-mass planet [Jang-Condell, 2006]. Even when R_t is as large as $\simeq 10$ AU, stirring of the disk by the tidal field and the thermal dissipation of spiral waves may inhibit planetesimal formation, as well as stabilize the disk against fragmentation [Nelson, 2000, Thébault et al., 2004, 2006]. In this case, it may be that neither the core-accretion picture nor gravitational instability [e.g., Boss, 2000] are accessible modes of giant planet formation. We adopt $R_t = 10$ AU ($a \lesssim 40$ AU for modest e) as a fiducial upper limit for which Jovian planet formation is significantly perturbed and perhaps strongly inhibited. This provides a simple theoretical definition of a close binary that roughly matches our observational measure.

A handful of planets in binaries with $a \lesssim 20$ AU have already been discovered (see Table 1). The tightest of these systems [HD 188753 Konacki, 2005b] has a periastron separation of only $\simeq 6$ AU, which seems severely at odds with the conventional lore on Jovian planet formation. Pfahl [2005] and Portegies Zwart and McMillan [2005] suggested that the planetary host star may have been acquired in a dynamical exchange interaction in a star cluster *after* the planet formed, thus circumventing the complicating factors listed above. As most stars are born in clustered environments, one wonders how often dynamics can account for planets in close binaries. This idea was explored in Pfahl and Muterspaugh [2006], where it was found that exchange interactions can account for only $\sim 0.1\%$ of close binaries hosting planets. However, the (admittedly small) sample of systems in Table 1 seems to indicate that a larger fraction of $\sim 1\%$ of close binaries harbor giant planets (see Pfahl & Muterspaugh 2006 for details), and perhaps planets do somehow form frequently in these hostile environments. It crucial that we begin to develop a census of planets in close binaries in order to test the different theories about planet formation and dynamics.

Close Binaries with Planets					
Object	a_b (AU)	e	M_1/M_2	R_t (AU)	Refs
HD 188753	12.3	0.50	1.06/1.63	1.3	1
γ Cephei	18.5	0.36	1.59/0.34	3.6	2, 3
GJ 86	~ 20		0.7/1.0	~ 5	4, 5, 6
HD 41004	~ 20		0.7/0.4	~ 6	7
HD 196885	~ 25		1.3/0.6	~ 7	8

Table 1: When no eccentricity is given, only the projected binary separation is known. M_1/M_2 is the planetary host mass divided by companion mass. In HD 188753, the secondary is a binary with semimajor axis 0.67 AU. In GJ 86, the secondary is a white dwarf; to estimate the tidal truncation radius R_t , an original companion mass of $1M_\odot$ is assumed. (1) Konacki [2005b]; (2) Campbell et al. [1988] (3) Hatzes et al. [2003]; (4) Queloz et al. [2000] (5) Mugrauer and Neuhäuser [2005] (6) Lagrange et al. [2006] (7) Zucker et al. [2004] (8) Chauvin et al. [2006]

2.2.1 PHASES Astrometry

The dualstar astrometry method can be modified for use when the binaries are so close that the individual telescopes of an interferometer cannot resolve the pair [Lane and Muterspaugh, 2004]. The interferometer itself over-resolves the binary, as in Fig. 1; its high spatial resolution then allows for precision astrometric measurements.

In this mode, the small separation of the binary results in both components being in the field of view of a single interferometric beam combiner. The fringe positions are measured by modulating the instrumental delay with an amplitude large enough to record both fringe packets.

However, since the fringe position measurement of the two stars is no longer truly simultaneous it is possible for the atmosphere to introduce path-length changes (and hence positional error) in the time between measurements of the separate fringes. To reduce this effect, a fraction of the incoming starlight is redirected to a separate beam-combiner. This beam-combiner is used in a “fringe-tracking” mode [Shao and Staelin, 1980, Colavita et al., 1999] where it rapidly (10 ms) measures the phase of one of the starlight fringes, and adjusts the internal delay to keep that phase constant. The fringe tracking data is used both in real-time as a feed-back servo, after

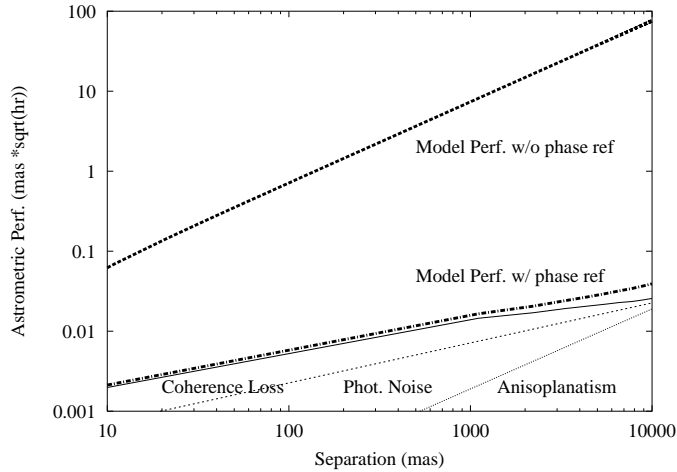


Figure 5: The expected narrow-angle astrometric performance in mas for the phase-referenced fringe-scanning approach, for a fixed delay sweep rate, and an interferometric baseline of 110 m. Also shown is the magnitude of the temporal loss of coherence effect in the absence of phase referencing, illustrating why stabilizing the fringe via phase referencing is necessary.

which a small residual phase error remains, and in post-processing where the measured residual error is applied to the data as a feed-forward servo. This technique—known as phase referencing—has the effect of stabilizing the fringe measured by the astrometric beam-combiner. For this observing mode, laser metrology is only required between the two beam combiners through the location of the light split (which occurs after the optical delay has been introduced), rather than throughout the entire array. Without phase referencing, the astrometric precision obtainable is a factor of a hundred worse; see Fig. 5.

To analyze the data, a double fringe packet based on Eq. 1 is then fit to the data, and the differential optical path between fringe packets is measured. A grid in differential right ascension and declination over which to search is constructed. For each point in the search grid the expected differential delay is calculated based on the interferometer location, baseline geometry, and time of observation for each scan. A model of a double-fringe packet is then calculated and compared to the observed scan to derive a χ^2 value; this is repeated for each scan, co-adding all of the χ^2 values associated with that point in the search grid. The final χ^2 surface as a function of differential R.A.

and declination is thus derived. The best-fit astrometric position is found at the minimum- χ^2 position, with uncertainties defined by the appropriate χ^2 contour—which depends on the number of degrees of freedom in the problem and the value of the χ^2 -minimum. The final product is a measurement of the apparent vector between the stars and associated uncertainty ellipse. Because the data were obtained with a single-baseline instrument, the resulting error contours are very elliptical, with aspect ratios that sometimes exceed 10:1.

The Palomar High-precision Astrometric Search for Exoplanet Systems (PHASES) program uses this technique to monitor ~ 50 binaries to search for substellar companions. κ Pegasi is a well-known, nearby triple star system. It consists of a “wide” pair with semi-major axis 235 mas (8.14 AU), one component of which is a single-line spectroscopic binary (semi-major axis 2.5 mas, physical separation 0.087 AU; Fig. 6). The perturbation due to the unseen (faint) short-period component is evident; similar sized perturbations with longer orbital periods would indicate the presence of planetary companions. Figure 7 shows the mass-period phase space in which PHASES observations show companions do not exist in face-on, circular orbits in the 13 Pegasi system.

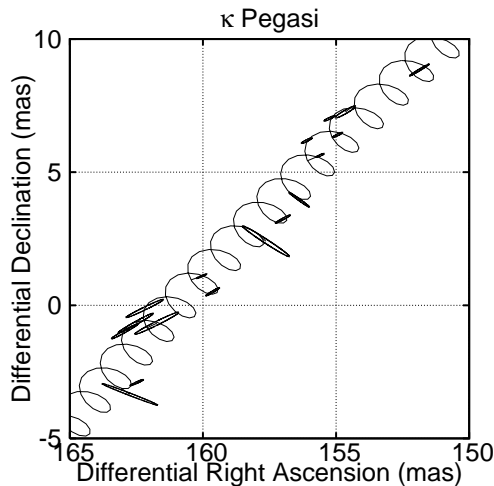


Figure 6: The visual orbits of κ Pegasi showing perturbations by the third component. The spiral line represents the apparent motion of the short-period pair’s center of light; the ellipses represent the 1σ uncertainties for PHASES measurements.

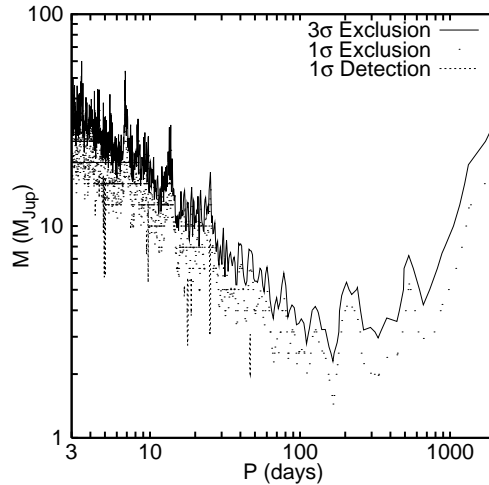


Figure 7: The 13 Pegasi Mass-Period companion phase space shows PHASES observations can rule out tertiary objects as small as two Jupiter masses. A few mass-period combinations introduce slight improvements over the single-Keplerian model, but none of these are more significant than 1.7σ , and are probably not astrophysical in origin. There is a long period cutoff in sensitivity due to the finite span of the observations. Similar detection limits have recently been published on other PHASES targets [Muterspaugh et al., 2006].

2.2.2 Radial Velocities

In the case when a composite spectrum of a binary star is observed, the classical approach with the iodine cell (described in section 2.1.2) cannot be used since it is not possible to observationally obtain two separate template spectra of the binary components. To resolve this problem, one can proceed as follows. First, one always takes two sequential exposures of each (binary) target—one with and the other without the cell. This is contrary to the standard approach for single stars where an exposure without the cell (a template) is taken only once. This way one obtains an instantaneous template that is used to model only the adjacent exposure taken with the cell. Next, one performs the usual least-squares fit and obtain the parameters described in eq. 8. Obviously, the derived Doppler shift, $\Delta\lambda_i$ (where i denotes the epoch of the observation), carries no meaning since each time a different template is used. Moreover, it describes a Doppler "shift" of a composed spectrum that

is typically different at each epoch. However, the parameters—in particular the wavelength solution and the parameters describing PSF—are accurately determined and can be used to extract the star spectrum, $I_{obs}^{*,i}(\lambda)$, for each epoch i , by inverting the eq. 8:

$$I_{obs}^{*,i}(\lambda) = [I_{obs}^i(\lambda) \otimes^{-1} PSF^i]/T_{I_2}(\lambda), \quad (12)$$

where \otimes^{-1} denotes deconvolution, and PSF^i represents the set of parameters describing PSF at the epoch i . Such a star spectrum has an accurate wavelength solution, is free of the I_2 lines and the influence of a varying PSF. In the final step, the velocities of both components of a binary target can be measured with the well know two-dimensional cross-correlation technique TODCOR [Zucker and Mazeh, 1994] using as templates the synthetic spectra derived with the ATLAS 9 and ATLAS 12 programs [Kurucz, 1995] and matched to the observed spectrum, $I_s(\lambda)$. The formal errors of the velocities can be derived from the scatter between the velocities from different echelle orders or using the formalism of TODCOR [Zucker and Mazeh, 1994]. The technique currently produces RVs of binary stars with an average precision of 20 m s^{-1} [Konacki, 2005a]. Improvements to the technique are being introduced to reach the level below 10 m s^{-1} .

With the iodine technique Konacki [2005a] has initiated the first RV survey for circumprimary or circumsecondary planets of binary or multiple stars (mainly hierarchical triples). The survey’s sample of ~ 450 binaries (northern and southern hemisphere) was selected based on the following criteria. (1) The apparent separation of the components had to be smaller than the width of the slit (e.g., 0.6 arcseconds for Keck-I/HIRES) to avoid possible systematic effects. Such systems will remain unresolved under most seeing conditions. (2) The brightness ratio between the components should not be too large (at the order of 10 or less) to be able to clearly identify spectra of both components. (3) The orbits of the binaries should be well known to constitute a firm ground on which one can discuss possible detection (or lack) of planets and substellar companions in the context of the binary characteristics. All these requirements could be satisfied by targeting a subset of speckle binaries that have determined orbits from the Catalog of Orbits of Visual Binary Stars [Hartkopf et al., 2001], containing 1700 binaries, of which 1300 have projected semi-major axes smaller than 1 arcsecond. The sample is sufficiently large to produce meaningful statistics. Also, such binaries have been ignored by previous RV studies.

The survey was initiated in 2003 at the Keck-I/HIRES and so far has covered about 50% of the northern hemisphere target sample, of which ~ 150 stars have been observed at least twice. In July 2005, the first candidate planet in a triple star system HD 188753 was announced [Konacki, 2005b]. A few more candidates as well as HD 188753 are currently being scrutinized. In the course of the Keck survey, a dozen of new triple star systems with the third bodies in the low-mass star or even brown dwarf regime have been also identified and will be published in the near future.

2.2.3 Eclipse Timing

Should a binary happen to be oriented with its orbital plane in the line of sight, it will exhibit eclipses as one star passes in front of another. For a binary with separation wide enough to allow for stable planetary systems to exist around just one component, the probability of such an alignment is extremely small, and very few targets are accessible. However, should one find such a fortunate happenstance, one can detect the planetary companions by precision timing of the eclipses. Clearly, this method has no direct analog for single systems.

This method can detect S-type planets or similarly moons of transiting planets. For this evaluation it is assumed that the depth of the planet (or moon) eclipse is sufficiently small as to be ignored (in such a detection, one could then reevaluate light curves to look for such transit signals) and the binary orbit is circular. The velocity of the binary orbit and the offset of the star-planet CM from that of the star by itself determines the timing variation observed as

$$\begin{aligned}
 \Delta t &= x_{CM}/v_b \\
 &= \left(\frac{a_p \sin \phi M_p}{M_2 + M_p} \right) \left(\frac{P_b}{2\pi a_b} \right) \\
 &\approx 57 \text{ seconds} \times (P_b/\text{month}) \frac{a_p}{(a_b/7)} \frac{(M_p/M_J)}{(M_2/M_\odot)} \sin \phi \quad (13)
 \end{aligned}$$

where M_2 is the mass of star 2 (or the transiting planet, assumed to host the S-type companion), M_p is the mass of the S-type object orbiting M_2 , ϕ is angle between the planet's orbital angular momentum vector and the direction of motion of the host star during eclipse, and P_b is the period of the binary orbit. The timing delays due to orbit of M_2 about the M_2 - M_p

CM. The factor of 7 appears in the final form is an approximate criteria for stability, that the planet semimajor axis is 7 times smaller than that of the binary (this factor varies by the system, and can be determined through detailed simulations); the above is thus an upper limit for the timing effect. Converting the semimajor axis to orbital periods,

$$\begin{aligned}\Delta t &\approx 41 \text{ seconds} \times (P_b/\text{month})^{\frac{1}{3}} (P_p/\text{day})^{\frac{2}{3}} \frac{M_p/M_J}{\left(M_b^{\frac{1}{3}} M_2^{\frac{2}{3}}\right) / M_\odot} \sin \phi \\ &\approx 65 \text{ seconds} \times (P_b/\text{month})^{\frac{1}{3}} (P_p/\text{day})^{\frac{2}{3}} \frac{M_p/M_J}{M_b/M_\odot} \sin \phi\end{aligned}\tag{14}$$

where $M_b = M_1 + M_2 + M_p$. The final form assumes $M_1 \approx M_2$, in which case the maximum stable planet period is a thirteenth that of the binary period, implying days and months are the natural units for each respectively (S-type planets cannot exist in much shorter period systems, and longer period systems are even less likely to show eclipses). The equivalent relationship for a moon orbiting an eclipsing Jupiter is

$$\Delta t \approx 13.3 \text{ seconds} \times (P_b/\text{month})^{\frac{1}{3}} (P_p/\text{day})^{\frac{2}{3}} \frac{M_p/M_\oplus}{(M_b/M_\odot)^{\frac{1}{3}} (M_2/M_J)^{\frac{2}{3}}} \sin \phi\tag{15}$$

where now the b subscript refers to the star-Jupiter analog system and p to the Jupiter analog's moon.

The precision with which eclipse minima can be timed is derived using standard χ^2 fitting techniques. Assume a photometric data set $\{y_i\}$ occurring at times $\{t_i\}$ with measurement precisions $\{\sigma_i\}$, and a model photometric light curve of flux $F(t - t_0)$. The corresponding intensity is $I(t - t_0) = fF(t - t_0)\pi D^2 \Delta t/4$, where f ($0 \leq f \leq 1$) is the fractional efficiency and throughput of the telescope, D is the telescope diameter, and Δt is the sample integration time. ($F(t - t_0)$ might be determined to high precision by observing multiple eclipse events.) The fit parameter t_0 is uncertain by an amount equal to the difference between the value for which χ^2 is minimized

and that for which it is increased by one: $1 + \chi^2(t_0) = \chi^2(t_0 + \sigma_{t_0})$,

$$\begin{aligned}
1 + \sum_{i=1}^N \left[\frac{y_i - I(t_i - t_0)}{\sigma_i} \right]^2 &= \sum_{i=1}^N \left[\frac{y_i - I(t_i - t_0 - \sigma_{t_0})}{\sigma_i} \right]^2 \\
&\approx \sum_{i=1}^N \left[\frac{y_i - I(t_i - t_0) - \left(\frac{\partial I(t)}{\partial t} \right)_{t=t_i - t_0} \sigma_{t_0}}{\sigma_i} \right]^2 \\
&= \sum_{i=1}^N \left(\left[\frac{y_i - I(t_i - t_0)}{\sigma_i} \right]^2 + \left[\frac{\left(\frac{\partial I(t)}{\partial t} \right)_{t=t_i - t_0} \sigma_{t_0}}{\sigma_i} \right]^2 - 2 \frac{\left(\frac{\partial I(t)}{\partial t} \right)_{t=t_i - t_0} [y_i - I(t_i - t_0)] \sigma_{t_0}}{\sigma_i^2} \right).
\end{aligned}$$

Because t_0 is the minimizing point, the first derivative of χ^2 at t_0 is zero, giving

$$\left(\frac{\partial \chi^2(t)}{\partial t} \right)_{t=t_0} = 2 \sum_{i=1}^N \frac{\left(\frac{\partial I(t)}{\partial t} \right)_{t=t_i - t_0} (y_i - I(t_i - t_0)) \sigma_{t_0}}{\sigma_i^2} = 0. \quad (16)$$

Rearrangement of terms leads to

$$\sigma_{t_0} = \frac{1}{\sqrt{\sum_{i=1}^N \left(\frac{\left(\frac{\partial I(t)}{\partial t} \right)_{t=t_i - t_0}}{\sigma_i} \right)^2}} \approx \frac{\sigma_I}{\sqrt{\sum_{i=1}^N \left(\frac{\partial I(t)}{\partial t} \right)_{t=t_i - t_0}^2}}.$$

An eclipse of length τ is approximated as a trapezoid-shape light curve (see Figure 8) with maximum and minimum photon fluxes F_0 and $F_0(1 - h/2)$ (h is a dimensionless positive number producing an eclipse depth of $hF_0/2$; in the case of a faint secondary, h is roughly twice the ratio of the squares of the stellar radii, $2R_2^2/R_1^2$). The ingress and egress are each assumed to be of length $k\tau/2$ ($k \approx 2R_2/(R_1 + R_2)$ is unity in the case of an eclipsing binary with components of equal size, when the trapezoid becomes a ‘‘V’’-shape). In functional form, this model is:

$$F(t-t_0) = \begin{cases} F_0 & t - t_0 \leq -\tau/2 \\ F_0(1 - ht/(k\tau) - h/(2k)) & -\tau/2 \leq t - t_0 \leq -\tau/2 + k\tau/2 \\ F_0(1 - h/2) & -\tau/2 + k\tau/2 \leq t - t_0 \leq \tau/2 - k\tau/2 \\ F_0(1 + ht/(k\tau) - h/(2k)) & \tau/2 - k\tau/2 \leq t - t_0 \leq \tau/2 \\ F_0 & \tau/2 \leq t - t_0 \end{cases} \quad (17)$$

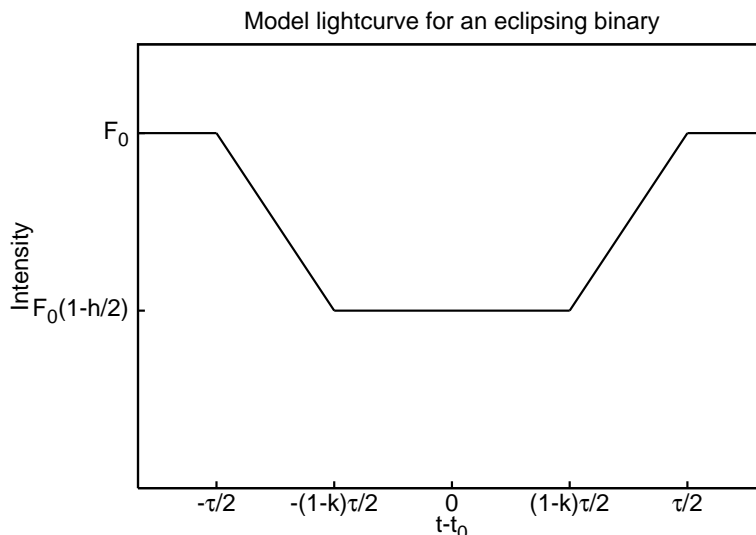


Figure 8: Eclipsing binary model light curve.

(also, see Figure 8).

Only the portions of the light curve during ingress and egress have nonzero $\frac{\partial F(t)}{\partial t}$ (in more accurate models, the light curve slope will be nonzero but small in other regions, and will not contribute much to the sum); this slope is $\left| \frac{\partial F(t)}{\partial t} \right| = hF_0 / (k\tau)$.

The number of data points contributing to the sum is thus $N = gk\tau/\Delta t$, where $0 \leq g \leq 1$ is the fraction of the eclipse observed (and also accounts for the fraction of time lost to, e.g., camera readout) and Δt is the integration time for each measurement.

The measurement noise σ_I is given by

$$\sigma_I = \left(I + \sigma_{sc}^2 + I_{bg} + n_{dark}\Delta t + \sigma_{rn}^2 \right)^{\frac{1}{2}} \quad (18)$$

where $I_{bg} = fF_{bg}\pi D^2\Delta t/4$ is the sky background, n_{dark} is detector dark current, σ_{rn} is detector read noise, and σ_{sc} is scintillation noise given by Young [1967] as

$$\sigma_{sc} = 0.09I (D/1 \text{ cm})^{-2/3} X e^{-h/(8000 \text{ m})} / (2\Delta t/1 \text{ second})^{\frac{1}{2}} \quad (19)$$

$$\approx 0.003I (D/1 \text{ m})^{-2/3} / (\Delta t/1 \text{ second})^{\frac{1}{2}} \quad (20)$$

where X is the airmass and h is the altitude of the observatory. The drop in noise during eclipse is ignored (a factor less than ≈ 1.4) and equation 18 is

combined with equation 17 to obtain an overall timing precision (in seconds) of

$$\begin{aligned}\sigma_{t_0} &= \sqrt{\frac{k(\tau/1 \text{ second})}{gh^2} \left(\frac{4}{fF_0\pi(D/1 \text{ m})^2} + \frac{9 \times 10^{-6}}{(D/1 \text{ m})^{4/3}} + \frac{\pi D^2 f F_{bg}/4 + n_{dark} + \sigma_{rn}^2/(\Delta t/1 \text{ second})}{f^2 F_0^2 \pi^2 (D/1 \text{ m})^4 / 16} \right)^{\frac{1}{2}}} \\ &\approx 0.18 \text{ seconds} \times \sqrt{\frac{k(\tau/1 \text{ hr})}{fgh^2} \left(\frac{10^{(V-12)/2.5}}{(D/1 \text{ m})^2} + \frac{f}{(D/1 \text{ m})^{4/3}} \right)^{\frac{1}{2}}}.\end{aligned}\quad (21)$$

The final term in the first line (associated with dark current, read noise, and background) is generally smallest and will be ignored. In most cases, the second term—associated with scintillation—is dominant (though zero in the case of space-based observatories). The exponent of $(V - 12)/2.5$ shows that for meter-sized telescopes, photon noise is only dominant for stars fainter than twelfth magnitude.

Systematic and astrophysical noise sources may have effects that limit the actual precisions achieved. Mass transfer between stars can cause drifts in orbital periods. Variations of this type are non-periodic, distinguishing them from companion signals. Applegate [1992] has shown that gravitational coupling to the shapes of magnetically active stars can cause periodic modulations over decade timescales. This mechanism requires the star to be inherently variable; false positives can be removed using the overall calibrations of photometric data. It is possible that star spots will have large effects on timing residuals that are particularly difficult to calibrate [Watson and Dhillon, 2004]. Due to orbit-rotation tidal locking, the effect of a starspot on the light curve can be detected from the light curves of several orbits, and starspot fitting potentially can remove the timing biases introduced.

The timescale for eclipses of such long period binaries is of the order of 12 hours. Comparing eqs. 14 and 21, one finds that S-type planets with periods of a few days can be detected around either star in eclipsing binaries with month-long periods if they mass more than

$$M_p/M_{\oplus} \gtrsim 3 \frac{(M_b/M_{\odot})}{(P_b/\text{month})^{\frac{1}{3}} (P_p/\text{day})^{\frac{2}{3}}} \sqrt{\frac{k(\tau/12 \text{ hr})}{fgh^2} \left(\frac{10^{(V-12)/2.5}}{(D/1 \text{ m})^2} + \frac{f}{(D/1 \text{ m})^{4/3}} \right)^{\frac{1}{2}}}.\quad (22)$$

Eq. 21 indicates that a meter-class ground-based telescope can time a giant planet transit ($h \approx 0.02$, $k \approx 0.18$) to approximately 9.4 seconds in the regime where the photometric precision is dominated by scintillation noise, assuming a Jupiter sized planet orbiting a star of solar size and mass with

period of a month (implying 6-hour duration eclipses). This precision is sufficient to find Earth mass moons. For bright stars, space-based observatories offer even better precisions. Unfortunately, no transiting exoplanets with periods this long have yet been discovered.

Space-based photometric missions such as Kepler have as their primary goal the detection of Earth-like planets via transits of the planet across the star. However, such photometric events can be explained by other astrophysical phenomena, such as a transiting Jupiter blended with a background star, so these results may be unreliable. However, Earth-like moons of transiting Jupiters might be identified through timing, and it is possible to confirm the nature of such a system. In such a scenario, a transiting Jupiter can be positively confirmed by ground-based radial velocity observations. Once this has been established, variations in the transit times would be used to detect Earth-sized moons. Because these photometric missions have limited lifetimes (≈ 3 years), detections of moons are only possible for short period (few months or less) Jupiters, for which many transit events can be observed (unless a follow-up ground-based campaign is pursued with large telescopes). If the planet/moon are to be in the habitable zone, one must look for such systems around late-type (cool) stars. It is possible that such systems have the greatest likelihood of being habitable; tidal-locking of the Earth-sized moon to the Jupiter-like planet would ensure that the moon has day/night cycles and stabilize its rotational axis similar to the way in which the Earth's is stabilized by its own moon. Both of these conditions have been argued as favorable for life [see, for example, Laskar et al., 1993].

2.2.4 Observational Precisions

Figure 9 shows the companion masses one can detect for each method, assuming $20 \mu\text{as}$ ground-based astrometry, 20m s^{-1} RV, and 1 m ground-based photometric telescope for eclipse timing.

3 P-Type (Circumbinary) Planets

All the confirmed planets found in binary systems thus far are in S-type orbits. Discovery of circumbinary planets would constitute a new class of solar system, and would inspire new considerations to the interplay between system dynamics and planet formation.

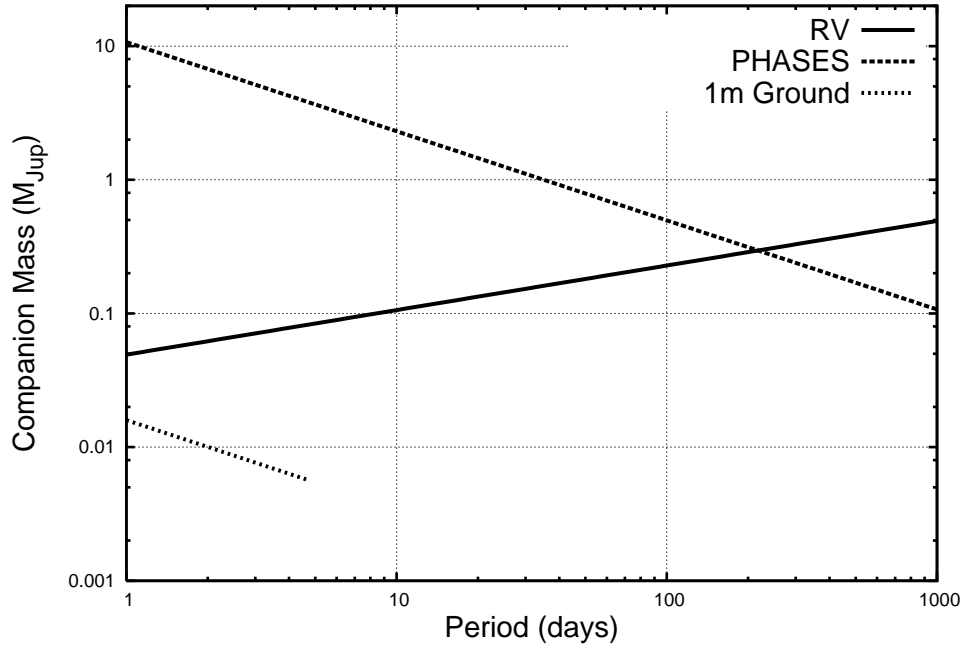


Figure 9: Sensitivity to S-Type planets in narrow binaries, comparing astrometric, radial velocity, and eclipse timing techniques. All calculations assume solar mass stars. The PHASES sensitivity assumes $20 \mu\text{as}$ precision and a distance to the system of 20 pc. Eclipse timing assumes a 1 m photometric telescope observing a $V = 10$ magnitude system with binary orbital period 2 months (longer period systems are even less likely to show eclipses); the eclipse timing sensitivity curve only extends to the region where planets are likely to have stable orbits.

3.1 Radial Velocities

A circumbinary planet will exhibit two indirect effects on the velocities of the stellar components of the system. First, the apparent system velocity will vary in a periodic manner due to the motion of the binary about the system barycenter. Second, the finite speed of light will cause apparent changes in the phase of the binary orbit. These effects may be detectable using modern observational techniques.

The first effect is that the binary will exhibit periodic changes in the apparent system velocity; this is the same effect as seen in a single star. However, it may be harder to detect for three reasons: (1) the binary system is usually more massive than a single star of the same magnitude, (2) extremely short-period planet orbits (to which system velocity measurements are most sensitive) are unstable around binaries, and (3) the presence of two sets of spectral lines may complicate the measurement, as in section 2.2.2. Equation 9 shows that a Jupiter mass planet with the shortest period stable orbit around a 10-day period binary causes a $2M_{\odot}$ binary to move about its barycenter by $\approx 40 \text{ m s}^{-1}$, with the amplitude decreasing as the square root of planet orbit semimajor axis. Radial velocity observations with the 20 m s^{-1} precision demonstrated with Konacki's method can detect Jupiter-like planets in orbits of size $\approx 4 \text{ AU}$ or less, down to the critically stable orbit.

The second observable effect is the additional light travel time as the binary system undergoes reflex motion caused by the planet. The magnitude of this effect is given by

$$\Delta t = 2 \frac{a_p M_p \sin i_p}{c M_b} = 0.95 \text{ seconds} \times \frac{(a_p/1 \text{ AU})(M_p/M_J) \sin i_p}{M_b/M_{\odot}}.$$

Following a similar derivation as that for finding the expected precision of eclipse timing, one finds the precision with which one can estimate the orbital phase of a binary based on radial velocity measurements is

$$\sigma_{\phi} = \frac{\sigma_{rv}}{\sqrt{\sum_i (\frac{\partial v_i}{\partial \phi})^2}}, \quad (23)$$

where σ_{rv} is the radial velocity measurement precision and $\frac{\partial v_i}{\partial \phi}$ is the derivative of the model radial velocity curve with respect to orbital phase, evaluated at times t_i . The timing precision corresponding to the phase precision derived is given by $\frac{\sigma_{\phi}}{2\pi} = \frac{\sigma_t}{P_b}$.

Approximating the binary orbit as circular, $v(t) \approx K \cos\left(\frac{2\pi t}{P_b} + \phi\right)$. If N measurements (each with two measured velocities, one for each star) are approximately evenly distributed in phase,

$$\sigma_\phi = \frac{\sqrt{2}\sigma_{rv}}{\sqrt{(2N-12)K}} \quad (24)$$

$$\sigma_t = \frac{P_b\sigma_{rv}}{\sqrt{2(2N-12)\pi K}}, \quad (25)$$

where 12 is the number of degrees of freedom for the model.

If the lines from both stars are observed, the effective K is $K_1 + K_2$ and the resulting (1σ) minimum detectable mass is thus

$$M_p = 41.4M_J \times \frac{(\sigma_{rv}/20 \text{ m s}^{-1})(P_b/10 \text{ days})^{4/3}(M_b/M_\odot)^{2/3}}{\sqrt{2N-12} \sin i_b \sin i_p (a_p/1 \text{ AU})}, \quad (26)$$

where i_b and i_p are the inclinations of the binary and planet orbits, respectively. Twenty-five 20 m s^{-1} radial velocity measurements of the “prototypical” system could detect moderate-mass brown dwarfs ($\approx 30M_J$) at critical orbit. Objects at the planet/brown dwarf threshold of $13 M_J$ are only detectable in orbits larger than 0.82 AU around a ten-day binary of sunlike stars. Alternatively, if only one set of lines are observed, the resulting expression is

$$M_p = 41.4M_J \times \left(1 + \frac{M_1}{M_2}\right) \frac{(\sigma_{rv}/20 \text{ m s}^{-1})(P_b/10 \text{ days})^{4/3}(M_b/M_\odot)^{2/3}}{\sqrt{N-11} \sin i_b \sin i_p (a_p/1 \text{ AU})}, \quad (27)$$

where M_1 is the mass of the star whose lines are observed, and M_2 is that of the faint star.

High precision radial velocity observations are only possible on slowly rotating ($v \sin i < 10 \text{ m s}^{-1}$) stars; measurements of more rapidly rotating stars are limited by line broadening to levels worse than the nominal 20 m s^{-1} that has been referenced by this work. This effect is particularly important for finding planets around short-period binaries, in which the stars’ rotation rates are often tidally locked to the binary orbital period; these rotation rates limit the observed precisions for systems with periods approximately five days or less.

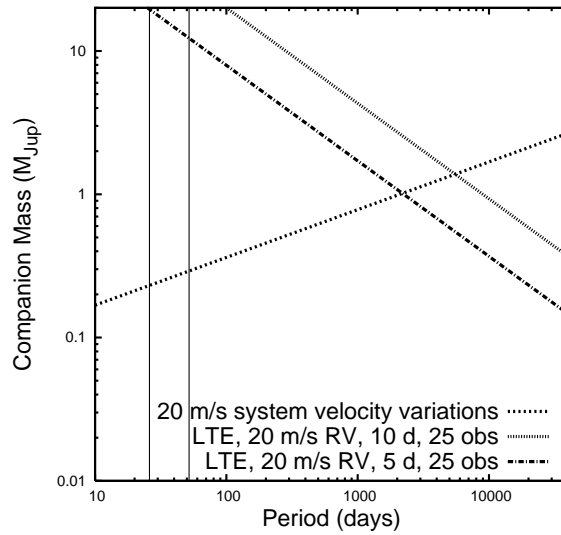


Figure 10: Sensitivity of radial velocity measurements to circumbinary planets. The two vertical lines at the left represent the approximate critical orbits around 5-day (to the left) and 10-day period binaries; shorter period companions have unstable orbits. Stars whose rotation rates are tidally locked to orbital periods less than about 5 days show sufficient rotational line broadening to prevent 20 m s^{-1} radial velocity precisions. The calculations assume the binary consists of two stars each massing $1 M_{\odot}$.

3.2 Eclipse Timing

It has long been recognized that periodic shifts in the observed times of photometric minima of eclipsing binaries can indicate the presence of an additional component to the system (see, for example, Woltjer [1922], Irwin [1952], Frieboes-Conde and Herczeg [1973], Doyle et al. [1998]). The amplitude of the effect is given by eq. 23. As with RV measurements, there is a mass/inclination ambiguity; the following derivation assumes no correlation between binary and planet inclinations.

Dividing the precision of an individual measurement by $N_{obs} - 6$ (where N_{obs} is the number of eclipses observed and there are 6 parameters to a timing perturbation fit, two periods and the eccentricity, angle of periastron, epoch of periastron, and mass ratio of the wide pair), converting F_0 to V magnitude, and combining eq. 21 with that for the timing effect of reflex motion (eq. 23) gives a minimum detectable companion mass of

$$M_p = 0.19 M_J \times \sqrt{\frac{k (\tau/1 \text{ hr})}{f g h^2 (N_{obs} - 6)}} \frac{M_b/M_\odot}{(a_p/1 \text{ AU}) \sin i_p} \left(\frac{10^{(V-12)/2.5}}{(D/1 \text{ m})^2} + \frac{f}{(D/1 \text{ m})^{4/3}} \right)^{\frac{1}{2}}. \quad (28)$$

One might also inquire about the sensitivity of this technique to outer planets in systems comprised of a single star and a transiting “hot” Jupiter. In this case, $h \approx 2R_p^2/R_{star}^2 \approx 0.02$ and $k \approx 2R_p/(R_{star} + R_p) \approx 0.18$, the “binary” is half as massive, and the eclipse duration is half as long. The companion sensitivity drops by a factor of 8, and the technique is (barely) in the range of detecting additional companions of planet mass. However, for the typically $V = 10$ magnitude transiting planet systems being discovered, 3 m s^{-1} radial velocity observations are more sensitive than half-meter telescope transit timing for companions with periods up to 60 years; even for observatories such as HST and SOFIA (for which scintillation noise is small or zero), this transition occurs at 15 year period companions.

It should be noted that the above description does not account for the possibility of resonant orbits, for which timing perturbations can be greatly enhanced by many-body dynamics—we have assumed independent Keplerian orbits for the subsystems. Resonant effects on timing perturbations have been considered by Holman and Murray [2005], Agol et al. [2005].

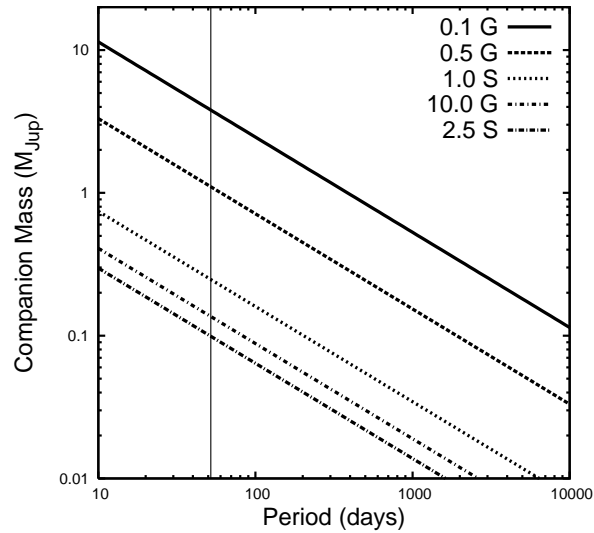


Figure 11: Sensitivity of eclipse timing measurements to circumbinary planets. The vertical line represents the approximate critical orbit around a 10-day period binary. The calculations assume the binary consists of two stars each massing $1 M_{\odot}$, 6 hour eclipses, $N_{obs} = 25$ observations (150 total hours of data), $V = 10$ magnitudes, and $1-\sigma$ detections. From top to bottom, lines show sensitivity for $D = 0.1$ m on the ground, $D = 0.5$ m on the ground, $D = 1.0$ m in space (i.e. Kepler), $D = 10$ m on the ground, and $D = 2.5$ m in space (HST, SOFIA).

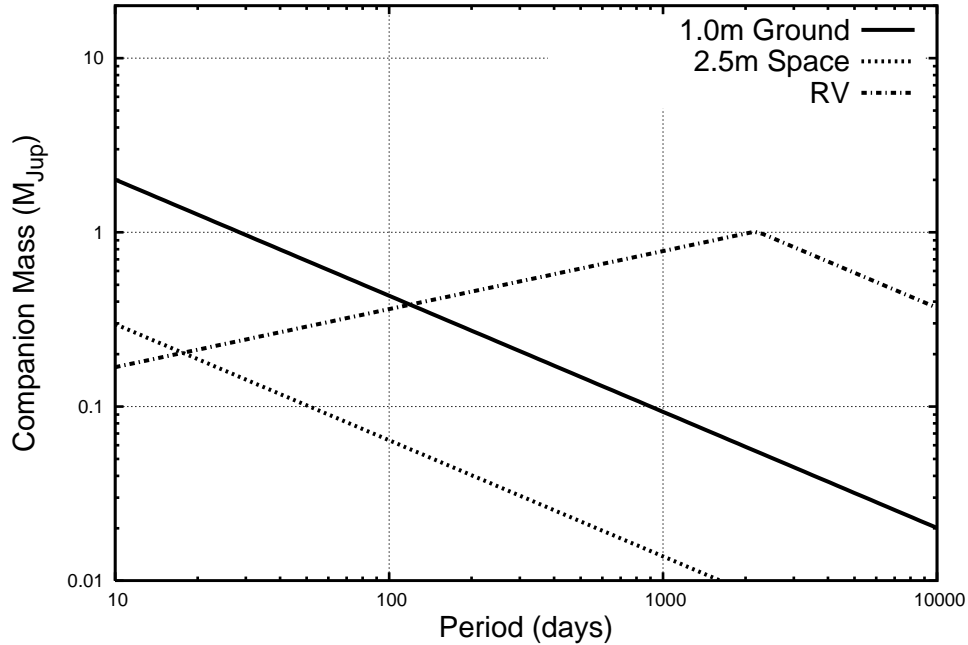


Figure 12: Sensitivity to circumbinary planets, comparing radial velocity and eclipse timing techniques. All calculations assume solar mass stars. RV assumes 20 m s^{-1} precision; both the system velocity and apparent period variation observables are included for the sensitivity curve, the latter assumes a 5 day binary orbital period. Eclipse timing assumes either a 1 m ground-based photometric telescope or 2.5 m space-based telescope (such as HST or SOFIA), observing a $V = 10$ magnitude system, and 25 observations.

3.3 Observational Precisions

Figure 12 compares the sensitivity of RV and eclipse timing to circumbinary planets.

References

- E. Agol, J. Steffen, R. Sari, and W. Clarkson. On detecting terrestrial planets with timing of giant planet transits. *MNRAS*, 359:567–579, May 2005. doi: 10.1111/j.1365-2966.2005.08922.x.

- J. H. Applegate. A mechanism for orbital period modulation in close binaries. *ApJ*, 385:621–629, February 1992.
- D. Benest. Planetary orbits in the elliptic restricted problem. I - The Alpha Centauri system. *A&A*, 206:143–146, November 1988.
- D. Benest. Planetary orbits in the elliptic restricted problem. II - The Sirius system. *A&A*, 223:361–364, October 1989.
- D. Benest. Stable planetary orbits around one component in nearby binary stars. II. *Celestial Mechanics and Dynamical Astronomy*, 56:45–50, June 1993.
- D. Benest. Planetary orbits in the elliptic restricted problem. III. The η Coronae Borealis system. *A&A*, 314:983–988, October 1996.
- D. Benest. Planetary orbits in the elliptic restricted problem. V.. The ADS 11060 system. *A&A*, 400:1103–1111, March 2003.
- A. P. Boss. Possible Rapid Gas Giant Planet Formation in the Solar Nebula and Other Protoplanetary Disks. *ApJ*, 536:L101–L104, June 2000. doi: 10.1086/312737.
- R. A. Broucke. Stable Orbits of Planets of a Binary Star System in the Three-Dimensional Restricted Problem. *Celestial Mechanics and Dynamical Astronomy*, 81:321–341, December 2001.
- R. P. Butler, G. W. Marcy, E. Williams, C. McCarthy, P. Dosanjuh, and S. S. Vogt. Attaining Doppler Precision of 3 M s⁻¹. *PASP*, 108:500–+, June 1996.
- B. Campbell, G. A. H. Walker, and S. Yang. A search for substellar companions to solar-type stars. *ApJ*, 331:902–921, August 1988. doi: 10.1086/166608.
- G. Chauvin, A. . Lagrange, S. Udry, T. Fusco, F. Galland, D. Naef, J. . Beuzit, and M. Mayor. Probing long-period companions to planetary hosts. VLT and CFHT near infrared coronagraphic imaging surveys. *A&A*, *in press*, astro-ph/0606166, June 2006.

- M. M. Colavita. Measurement of the Atmospheric Limit to Narrow Angle Interferometric Astrometry Using the Mark-III Stellar Interferometer. *A&A*, 283:1027–+, March 1994.
- M. M. Colavita, J. K. Wallace, B. E. Hines, Y. Gursel, F. Malbet, D. L. Palmer, X. P. Pan, M. Shao, J. W. Yu, A. F. Boden, P. J. Dumont, J. Gubler, C. D. Koresko, S. R. Kulkarni, B. F. Lane, D. W. Mobley, and G. T. van Belle. The Palomar Testbed Interferometer. *ApJ*, 510: 505–521, January 1999.
- S. Desidera, R. Gratton, R. Claudi, M. Barbieri, G. Bonanno, M. Bonavita, R. Cosentino, M. Endl, S. Lucatello, A. F. Martinez Fiorenzano, F. Marzari, and S. Scuderi. Searching for planets around stars in wide binaries. pages 119–126, February 2006.
- L. R. Doyle, H. Deeg, J. M. Jenkins, J. Schneider, Z. Ninkov, R. Stone, H. Gotzger, B. Friedman, J. E. Blue, and M. F. Doyle. Detectability of Jupiter-to-Brown-Dwarf-Mass Companions Around Small Eclipsing Binary Systems. In *ASP Conf. Ser. 134: Brown Dwarfs and Extrasolar Planets*, pages 224–+, 1998.
- R. Dvorak. Planetary orbits in double star systems. *Oesterreichische Akademie Wissenschaften Mathematisch naturwissenschaftliche Klasse Sitzungsberichte Abteilung*, 191:423–437, 1982.
- H. Frieboes-Conde and T. Herczeg. Period variations of fourteen eclipsing binaries with possible light-time effect. *A&AS*, 12:1–+, October 1973.
- W. I. Hartkopf, B. D. Mason, and C. E. Worley. Sixth catalog of orbits of visual binary stars. <http://www.ad.usno.navy.mil/wds/orb6/orb6.html>, 2001.
- A. P. Hatzes, W. D. Cochran, M. Endl, B. McArthur, D. B. Paulson, G. A. H. Walker, B. Campbell, and S. Yang. A Planetary Companion to γ Cephei A. *ApJ*, 599:1383–1394, December 2003. doi: 10.1086/379281.
- M. J. Holman and N. W. Murray. The Use of Transit Timing to Detect Terrestrial-Mass Extrasolar Planets. *Science*, 307:1288–1291, February 2005. doi: 10.1126/science.1107822.

- M. J. Holman and P. A. Wiegert. Long-Term Stability of Planets in Binary Systems. *AJ*, 117:621–628, January 1999.
- J. B. Irwin. The Determination of a Light-Time Orbit. *ApJ*, 116:211–+, July 1952.
- H. Jang-Condell. Constraints on the Formation of the Planet Around HD188753A. *ApJ*, *in press*, *astro-ph/050735*, July 2006.
- M. Konacki. Precision Radial Velocities of Double-lined Spectroscopic Binaries with an Iodine Absorption Cell. *ApJ*, 626:431–438, June 2005a. doi: 10.1086/429880.
- M. Konacki. An extrasolar giant planet in a close triple-star system. *Nature*, 436:230–233, July 2005b. doi: 10.1038/nature03856.
- R. L. Kurucz. The Kurucz Smithsonian Atomic and Molecular Database. pages 205–+, 1995.
- A. . Lagrange, H. Beust, S. Udry, G. Chauvin, and M. Mayor. New constrains on Gliese 86 B. *A&A*, *in press*, *astro-ph/0606167*, June 2006.
- B. F. Lane and M. W. Muterspaugh. Differential Astrometry of Subarcsecond Scale Binaries at the Palomar Testbed Interferometer. *ApJ*, 601:1129–1135, February 2004.
- B. F. Lane, M. M. Colavita, A. F. Boden, and P. R. Lawson. Palomar Testbed Interferometer: update. In *Proc. SPIE Vol. 4006, p. 452-458, Interferometry in Optical Astronomy, Pierre J. Lena; Andreas Quirrenbach; Eds.*, pages 452–458, July 2000.
- J. Laskar, F. Joutel, and P. Robutel. Stabilization of the earth’s obliquity by the moon. *Nature*, 361:615–617, February 1993.
- P. R. Lawson, editor. *Principles of Long Baseline Stellar Interferometry*, 2000.
- J. J. Lissauer. Planet formation. *ARA&A*, 31:129–174, 1993. doi: 10.1146/annurev.aa.31.090193.001021.
- G. W. Marcy and R. P. Butler. Precision radial velocities with an iodine absorption cell. *PASP*, 104:270–277, April 1992.

- M. Mugrauer and R. Neuhauser. Gl86B: a white dwarf orbits an exoplanet host star. *MNRAS*, 361:L15–L19, July 2005. doi: 10.1111/j.1745-3933.2005.00055.x.
- M. W. Muterspaugh, B. F. Lane, S. R. Kulkarni, B. F. Burke, M. M. Colavita, and M. Shao. Limits to Tertiary Astrometric Companions in Binary Systems. *ApJ*, 653, November 2006. doi: 10.1086/508743.
- A. F. Nelson. Planet Formation is Unlikely in Equal-Mass Binary Systems with $A \sim 50$ AU. *ApJ*, 537:L65–L68, July 2000.
- E. Pfahl. Cluster Origin of the Triple Star HD 188753 and Its Planet. *ApJ*, 635:L89–L92, December 2005. doi: 10.1086/499162.
- E. Pfahl and M. Muterspaugh. Impact of Stellar Dynamics on the Frequency of Giant Planets in Close Binaries. *ApJ*, 652:1694–1697, December 2006. doi: 10.1086/508446.
- B. Pichardo, L. S. Sparke, and L. A. Aguilar. Circumstellar and circumbinary discs in eccentric stellar binaries. *MNRAS*, 359:521–530, May 2005. doi: 10.1111/j.1365-2966.2005.08905.x.
- E. Pilat-Lohinger and R. Dvorak. Stability of S-type Orbits in Binaries. *Celestial Mechanics and Dynamical Astronomy*, 82:143–153, 2002.
- E. Pilat-Lohinger, B. Funk, and R. Dvorak. Stability limits in double stars. A study of inclined planetary orbits. *A&A*, 400:1085–1094, March 2003.
- S. F. Portegies Zwart and S. L. W. McMillan. Planets in Triple Star Systems: The Case of HD 188753. *ApJ*, 633:L141–L144, November 2005. doi: 10.1086/498302.
- D. Queloz, M. Mayor, L. Weber, A. Blécha, M. Burnet, B. Confino, D. Naef, F. Pepe, N. Santos, and S. Udry. The CORALIE survey for southern extra-solar planets. I. A planet orbiting the star Gliese 86. *A&A*, 354:99–102, February 2000.
- G. Rabl and R. Dvorak. Satellite-type planetary orbits in double stars - A numerical approach. *A&A*, 191:385–391, February 1988.
- M. Shao and M. M. Colavita. Potential of long-baseline infrared interferometry for narrow-angle astrometry. *A&A*, 262:353–358, August 1992.

- M. Shao and D. H. Staelin. First fringe measurements with a phase-tracking stellar interferometer. *Appl. Opt.*, 19:1519–1522, May 1980.
- P. Thébault, F. Marzari, H. Scholl, D. Turrini, and M. Barbieri. Planetary formation in the γ Cephei system. *A&A*, 427:1097–1104, December 2004. doi: 10.1051/0004-6361:20040514.
- P. Thébault, F. Marzari, and H. Scholl. Relative velocities among accreting planetesimals in binary systems: The circumprimary case. *Icarus*, 183:193–206, July 2006. doi: 10.1016/j.icarus.2006.01.022.
- E. Toyota, Y. Itoh, H. Matsuyama, S. Urakawa, S. Kimura, Y. Oasa, T. Mukai, and B. Sato. Search for Extrasolar Planets in Binary Systems. pages 8247–+, 2005.
- S. Udry, A. Eggenberger, M. Mayor, T. Mazeh, and S. Zucker. Planets in multiple-star systems: properties and detections. pages 207–214, August 2004.
- C. A. Watson and V. S. Dhillon. The effect of star-spots on eclipse timings of binary stars. *MNRAS*, 351:110–116, June 2004.
- J. Woltjer. On a special case of orbit determination in the theory of eclipsing variables. *Bull. Astron. Inst. Netherlands*, 1:93–+, June 1922.
- A. T. Young. Photometric error analysis. VI. Confirmation of Reiger’s theory of scintillation. *AJ*, 72:747–+, August 1967.
- S. Zucker and T. Mazeh. Study of spectroscopic binaries with TODCOR. 1: A new two-dimensional correlation algorithm to derive the radial velocities of the two components. *ApJ*, 420:806–810, January 1994. doi: 10.1086/173605.
- S. Zucker, T. Mazeh, N. C. Santos, S. Udry, and M. Mayor. Multi-order TODCOR: Application to observations taken with the CORALIE echelle spectrograph. II. A planet in the system HD 41004. *A&A*, 426:695–698, November 2004. doi: 10.1051/0004-6361:20040384.